J. Plasma Physics (1998), *vol.* 59, *part* 4, *pp.* 761–772. Printed in the United Kingdom
© 1998 Cambridge University Press

E × B guiding-centre motion in three electrostatic waves: statistics of separatrix crossings

B. WEYSSOW

Association EURATOM–Etat Belge sur la Fusion, Service de Physique Statistique, Plasmas et Optique Non Linéaire, Université Libre de Bruxelles, Campus Plaine CP 231, Boulevard du Triomphe, B-1050 Bruxelles, Belgium

(Received 4 September 1997 and in revised form 21 October 1997)

E × **B** guiding-centre (GC) motion in a special configuration of three low-frequency electrostatic waves can be considered as a paradigmatic Hamiltonian system for studying adiabatic motion and separatrix crossings. A peculiarity of this system is that a single initial condition gives rise to two stroboscopic phase-space trajectories. According to the classical Hamiltonian theory, the proportion of points on the stroboscopic trajectories is a function of the time evolution of the surfaces enclosed by the separatrices in the phase space. This behaviour is qualitatively observed in test-particle numerical experiments. The ability of numerical integration methods like the 'classical' fourth-order Runge–Kutta integration scheme or a third-order symplectic integrator to reproduce the statistics is analysed.

1. Introduction

Understanding of anomalous transport in tokamak plasmas is still a challenge for physicists. As is well known, only two limits in the frequency range of electrostatic instabilities can be studied analytically (using Gaussian approximations): in the low-frequency limit ($\omega < 1$), the traditional theory gives the Bohm scaling for the diffusion coefficient (see e.g. Dupree 1967), and in the high-frequency limit, it gives a quasilinear diffusion coefficient. Thus, if $\mathscr{A}$ is the dimensionless turbulence amplitude (see Appendix A), the diffusion coefficient in the low frequency limit (wave frequency much smaller than the guiding-centre rotation frequency) resulting from the Gaussian theory is $\mathscr{D}(\mathscr{A}) = \mathscr{A}^{\gamma}$, with $\gamma = 1$. More recently, this problem has been reconsidered by Isichenko and Horton (1991). They showed, on the basis of percolation theory, that the exponent γ should be smaller than one: $\gamma = 0.7$. Numerical experiments have given a critical exponent value between 0.7 and 0.8. Ottaviani (1992) obtained 0.8 with a set of 64 waves of random amplitudes, whereas Reuss and Misguich (1997) obtained 0.7 with turbulence spectrum defined on a limited wavelength range. This last result was recovered by Weyssow and De Leener (unpublished work) with a turbulence spectrum defined on a larger wavelength range. This type of diffusion, with non-integer exponent γ, was also observed in other numerical experiments (e.g. by Doxas *et al.* 1990).

https://doi.org/10.1017/S0022377898006679 Published online by Cambridge University Press

Despite the agreement between the percolation scaling law and the scaling deduced from the numerical experiments, questions concerning the percolation mechanism in Hamiltonian systems remain open. For exemple, the compatibility of the percolation theory with the Hamiltonian theory is questionable, since the shape of the trajectories (the fractal dimension) is the important quantity in the percolation theory but is not in the classical Hamiltonian formalism. Thus the possibility that a different type of diffusion appears beyond the percolation regime should be considered.

Our goal is thus twofold. First, we want to test the adiabatic limit of the Hamiltonian theory. To this end, we set up a Hamiltonian system whose behaviour is known analytically (one initial condition gives two stroboscopic trajectories in the phase space; the occupancy rates are evaluated using the adiabatic theory) and for which numerical simulations can easily be performed. In our view, the fact that the adiabatic theory applies is an indication that a new type of diffusion could exist. Indeed, in the Bohm scaling, the dimensional diffusion coefficient is independent of the frequency. In other words, the mean square displacement after a large number of periods for sufficiently small frequencies is inversely proportional to the frequency. In the adiabatic theory applied to single-frequency Hamiltonian systems, the whole dynamics is independent of the frequency, provided that the period is used as the unit of time. In this theory, the times for a separatrix crossing depend only on the temporal evolution of the surfaces of the domains enclosed by the separatrices (for a single-frequency potential this evolution is independent of the frequency); thus the occupancy rates of the stroboscopic trajectories are independent of the frequency. Thus, an extrapolation of this process to a diffusive system would give a dimensional diffusion coefficient (if it exists) proportional to the frequency.

Secondly, by comparing the statistics of the stroboscopic points of the adiabatic theory with the statistics obtained by the numerical simulations, we should be able to define a method for analysing analytically or numerically the dynamics guiding-centre over very long intervals of time. In this regard, we see at least two aspects of the problem that can be analysed with our choice of Hamiltonian. The first concerns the frequency below which the adiabatic theory eventually applies. This result, exported to the diffusion problem, should give the amplitude $\mathscr{A}$ at which the percolation scaling could start to be wrong. The second aspect is the justification of the linear relation between the time step of integration and the wave frequency that is frequently used in the numerical simulations devoted to the study of the diffusion. This linear relation between the time step of integration and the wave frequency is expected on different bases. Here, it is deduced from a graphical representation of the occupancy rates of the stroboscopic trajectories versus the frequency and the time step of integration.

In Sect. 1, we discuss the three-wave paradigmatic Hamiltonian and its asymptotic dynamics. In Sect. 2, we analyse the results of the numerical integration of the equations of motion and discuss the problems arising from the use of the numerical integration schemes: classical and symplectic. Finally, we give our conclusions. In Appendix B, we briefly explain the procedure for building a simplectic integrator and give the formula for the third-order symplectic integrator used in the numerical calculations.

https://doi.org/10.1017/S0022377898006679 Published online by Cambridge University Press

2. The three-wave Hamiltonian

The **E** × **B** Hamiltonian of a guiding centre (GC) in the three electrostatic waves and in a static and uniform magnetic field is as follows (Weyssow 1997):

$$H(x, y, t) = \sin[2\pi(x + \omega t)] + \sin[2\pi(y + \omega t)] + \sin[2\pi(x + y + \omega t)]. \tag{2.1}$$

It is a special case of a three-wave Hamiltonian (a more general three-wave Hamiltonian has been considered in another context by Misguich and Nakach 1991). The consequence of our choice for the wave amplitudes, wavelengths and wave frequencies is that the phase space comprises a static array of squares whose borders are made of uncrossable separatrices (indeed, we have $dy/dt = 0$ at $x = \pm 0.5$ and similarly in the y direction). The time dependence of the Hamiltonian appears in phase space through the motion of (two) oblique separatrices passing periodically through each square. This structure of phase space, as well as two GC trajectories (starting at ($x = y = 0.15$) and ($x = y = 0.005$)) of the frozen Hamiltonian (fixed time; here $t = 0$) are shown on Fig. 1. It is obvious from the previous discussion that this system does not allow for a study of a diffusion process: a GC in a square remains forever in that square. The system is, however, stochastic, with the degree of stochasticity depending on the wave frequency ω. For very large ω (the domain usually considered in the studies of the onset of stochasticity), the Hamiltonian can be approximated by a time-independent Hamiltonian obtained by applying an averaging procedure and the stochasticity sets in owing to the presence of higher-order terms, which become more and more important as the frequency is decreased. In the other limit, for very small frequencies (much smaller than the GC rotation frequency), the GC motion is also nearly integrable, and the theory of adiabatic invariants can be applied. In this case, the rules are as follows (Neistadt 1986; Weyssow 1997):

(1) the canonical action is very well conserved except at separatrix crossing times;

(2) the separatrix crossings are instantaneous events;

(3) the canonical action after a separatrix crossing depends on the evolution of the surfaces enclosed by the separatrices.

We shall only consider one of the squares (they are all the same; see Fig. 1). At an arbitrary time, this square is divided into three domains by two moving separatrices. In the low-frequency limit, the motion of a GC reduces to a succession of rotations around the elliptic point of one of the domains, followed by a jump into another domain, and so on. The canonical action defined by $s = \int y\,dx$ is an adiabatic invariant: $ds/dt \approx 0$. In the 'adiabatic limit', this action is conserved at all times except separatrix crossing times. Such events happen when the domain in phase space enclosing the GC has a surface area equal to the canonical action of the GC. From here on, the long-term dynamics is almost completely known: starting with a canonical action, the GC moves keeping this quantity constant until there is a separatrix crossing. The time at which this event happens is deduced from the evolution of the surfaces of the domains of the square. The remaining unknown is the change in the canonical action due to a separatrix crossing: in the 'adiabatic limit' and at the separatrix crossing time, the GC has a canonical action equal to the surface of one among two of the three domains of the square. Which is the new action is undecidable unless two domains have a decreasing surface area. This is

https://doi.org/10.1017/S0022377898006679 Published online by Cambridge University Press

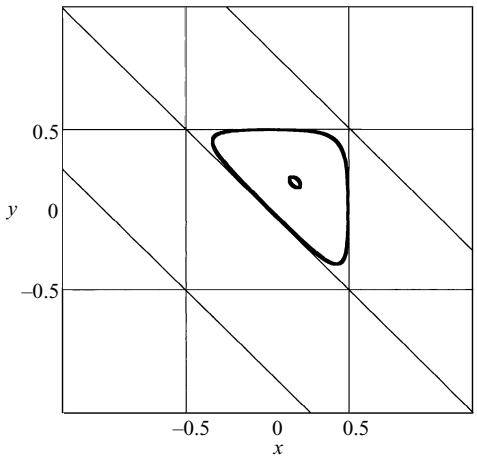


Figure 1. Phase space at time $t = 0$, showing the reference square, the moving separatrices and two trajectories of the frozen Hamiltonian

exactly where stochasticity sets in: the new canonical action can, in general (for our three-wave Hamiltonian), take two values. The occurrence of each value follows a statistical rule. For a GC to be captured by domain $i = 1$ or $i = 2$ or $i = 3$ in the square, the surface area s_i of this domain should be increasing: $ds_i/dt \geqslant 0$. The probability to be captured by domain i of the square can thus be deduced from the time derivative of the surfaces of the domains. Indeed, for a GC leaving domain i, the conservation law $ds/dt = 0$, where s is the total area of the square, can be rewritten as

$$1 = -\frac{ds_j}{dt} \Big/ \frac{ds_i}{dt} - \frac{ds_k}{dt} \Big/ \frac{ds_i}{dt}. \tag{2.2}$$

The probability for a GC leaving the domain i to be captured by domain j or domain k is thus

$$p_{ij} = -\frac{ds_j}{dt} \Big/ \frac{ds_i}{dt} \tag{2.3a}$$

or

$$p_{ik} = -\frac{ds_k}{dt} \Big/ \frac{ds_i}{dt} \tag{2.3b}$$

respectively, provided that these are positive quantities. A final analysis of the time evolution of the surfaces of the domain (periodic functions of the time) shows that an initial condition (a point in the square) gives rise to two closed stroboscopic trajectories that are also two distinct trajectories of the frozen Hamiltonian. The number of stroboscopic points on each trajectory is known from the probabilities defined hereabove.

The unusual characteristic of the three-wave Hamiltonian discussed here is that it gives a very simple but non-trivial dynamics in the low-frequency limit. This behaviour is best analysed by considering stroboscopic times, since, in this case, the phase-space plot of the GC motion shows two well-defined closed trajectories. We thus have, with this system, the possibility of analysing the onset of stochasticity from the low-frequency limit.

https://doi.org/10.1017/S0022377898006679 Published online by Cambridge University Press

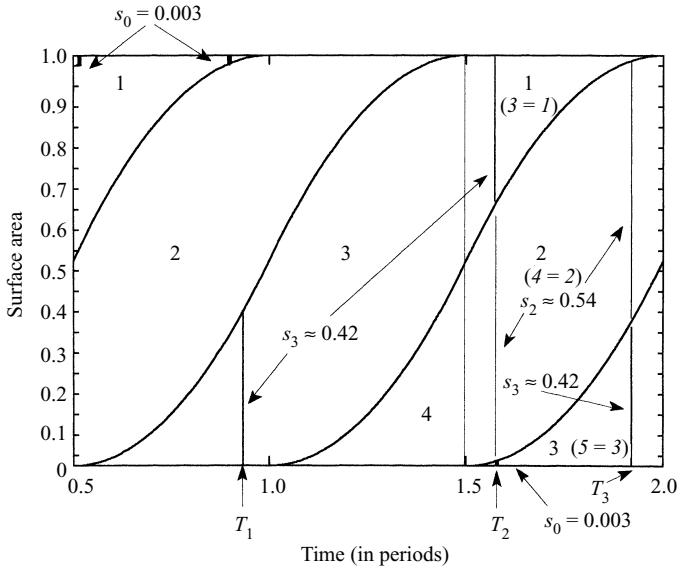


Figure 2. Time evolution of the areas of the surfaces enclosed by the separatrices in the square. Also shown are the times for separatrix crossings for a GC trajectory starting at $x = y = 0.15$ at time $t = 0$.

Our goal is to analyse the influence of a frequency change on the GC dynamics. For this study, we shall use two different numerical methods: the classical fourth-order Runge–Kutta method (Press *et al.* 1987) and a third-order symplectic method described in Appendix B (see B 6). For this study, we choose the initial point to be at $x = y = 0.15$ at time $t = 0$. The canonical action, evaluated using the RK4 for integrating the frozen Hamiltonian, is $s_1 \approx 0.0031$. When one domain of the square has this surface area, the square shows two other domains with surface areas $s_2 \approx 0.42$ and $s_3 \approx 0.57$. The trajectory in the frozen Hamiltonian that has canonical action equal to the surface area of the second domain passes through the point $x = y \approx 0.005$ (see Fig. 2).

3. Statistics

The trajectory of the GC starting at the position $x = y = 0.15$ can be followed from a drawing of the evolution of the surfaces of the three domains of the square. This evolution is shown on Fig. 2, where the areas of the three (occasionally two) domains of the square are plotted as functions of the time. The total surface area of the square is 1; the area of a domain at a given time is measured along a vertical line and is the distance between two S shaped curves or an S shaped curve and one of the horizontal lines (e.g. at time $t = 0$, the square is divided into two domains of equal surface area, 0.5). According to the rules defined in the previous section, a first half-period is used to transfer the initial condition from the position $x = y = 0.15$ to the position $x = y = -0.15$. A first separatrix crossing occurs shortly before the end of the second half-period (time T_1). At this time, the GC is captured by the domain having a surface area equal to $s = 0.42$. The new canonical action is thus equal to 0.42. At the end of the first period (the first stroboscopic time), the canonical action is thus 0.42 with probability 1. At time $t = 1 + 0.54$ (de-

https://doi.org/10.1017/S0022377898006679 Published online by Cambridge University Press

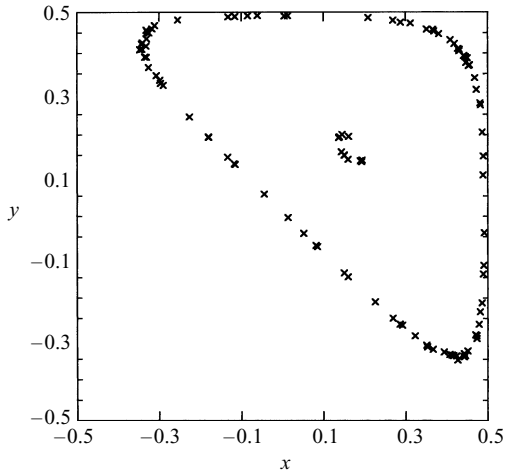


Figure 3. The two stroboscopic trajectories obtained with a fourth-order Runge–Kutta for a GC trajectory starting at $x = y = 0.15$ at time $t = 0$. The other parameters are $\omega = 0.00125$ and 3.2×10^6 integration steps per period. There are 11 points on the inner trajectory for 100 stroboscopic points.

noted T_2), the GC again crosses a separatrix. It can then be captured by any of the other two domains (denoted 2 and 3) of the square because they both have an increasing area. The canonical action could thus be 0.003 with probability $p_{13} \approx 0.09$, or it could be 0.57 with probability $p_{12} \approx 0.91$. If the latter case occurs, the GC will jump again shortly before the end of the second period (at time T_3), to give a canonical action equal to 0.42. In the former case, the canonical action 0.003 is conserved until the end of the second period. At the end of the second period, the GC has, with a probability 0.09, its initial canonical action or, with a probability 0.91, a 'conjugated' canonical action equal to 0.42. This analysis can be repeated for the third and following periods. All this process can be observed numerically by integrating the equations of motion (provided the frequency is small enough: less than $\omega = 0.01$). Figure 3 shows 100 stroboscopic points obtained by solving the equations of motion with a fourth-order Runge–Kutta. The two stroboscopic trajectories are clearly two trajectories of the frozen Hamiltonian. This result demonstrates that for small-enough wave frequency, the adiabatic theory is correct even for a system showing a large number of separatrix crossings. Furthermore, we see that the dynamics of the system, for a wave frequency going to zero, does not reduce to the dynamics of the frozen Hamiltonian, since in the former case we find two stroboscopic trajectories starting from only one initial condition. Thus the dynamics of a Hamiltonian system in the limit of vanishing frequency could be different from the dynamics of the frozen Hamiltonian. This is a counterexemple to the argument (e.g. by Gruzinov *et al.* 1990) used to prove the vanishing of the diffusion coefficient and saying that in the limit of very small frequency the $1\frac{1}{2}$-degree-of-freedom Hamiltonian system has one more invariant of motion and thus is integrable. In fact, in our case, this proposition is indeed true except at the times corresponding to instantaneous separatrix crossings. The next point in our programme is to investigate the effect of varying the frequency on the adiabatic dynamics. Our conclusions are based on two series of numerical experiments: one with a fourth-order Runge–Kutta integrator and one with a third-order symplectic

https://doi.org/10.1017/S0022377898006679 Published online by Cambridge University Press

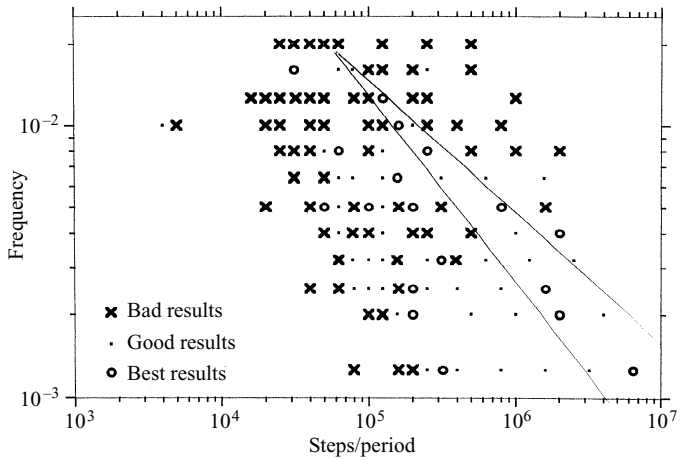


Figure 4. 'Quality' of the stroboscopic trajectories obtained with a fourth-order Runge–Kutta for a GC trajectory starting at $x = y = 0.15$ at time $t = 0$ and represented in the parameter space of wave frequency and integration time step.

integrator. The results are shown respectively in Figs 4 and 5. The figures gives the 'quality' of the integration of the equations of motion in terms of the wave frequency and the integration time step. In all cases, the equations of motions were integrated over 100 wave periods. We denote by 'bad' results those stroboscopic plots showing points far away from the adiabatic stroboscopic trajectories (e.g. in the bottom left corner). The remaining results are identified by a dot or by a circle. The circle is used for the 'best' results (those showing a minimum of dispersion about the adiabatic stroboscopic trajectories) in a series of stroboscopic plots obtained at fixed frequency and different values of the time step. An example of a 'best' result is given in Fig. 3. We first consider the results of the Runge–Kutta. The parameter space (frequency versus number of integration steps per period) shows regions with good results and regions with bad results. As expected, the bad results are due to too-large time steps, whereas good results are obtained in the domain of small wave frequency and small time step. The adiabatic limit holds for frequencies smaller than $\omega = 0.01$. In terms of the dimensionless amplitude $\mathscr{A}$ (defined in (A 8)), the adiabatic theory could hold for amplitudes larger than $\mathscr{A} = 1250$, which is a value much larger than considered up to now in numerical experiments on diffusion (see e.g. Reuss and Misguich 1997).

Less expected are the bad results in the central region of parameter space. The existence of this region implies that the only way to go from the lower right corner of the parameter space to the inside of the parameter space passing near to the 'good' results is to follow an oblique line of slope -0.7. We recall that in numerical simulations a slope of -1 is usually considered as a good choice: this is not the case in the present study – at least for the values of the time steps considered here. Along the line, the number of stroboscopic points forming the inner trajectory is almost constant, and is slightly larger than the expected value of 9/100 (about 10 for 100 stroboscopic points). Thus, for very small wave frequencies, the dynamics of the GC observed at stroboscopic times and along the line of slope -0.7 is (quasi) independent of the frequency.

The symplectic method behaves differently. From Fig. 5, we see that good results

https://doi.org/10.1017/S0022377898006679 Published online by Cambridge University Press

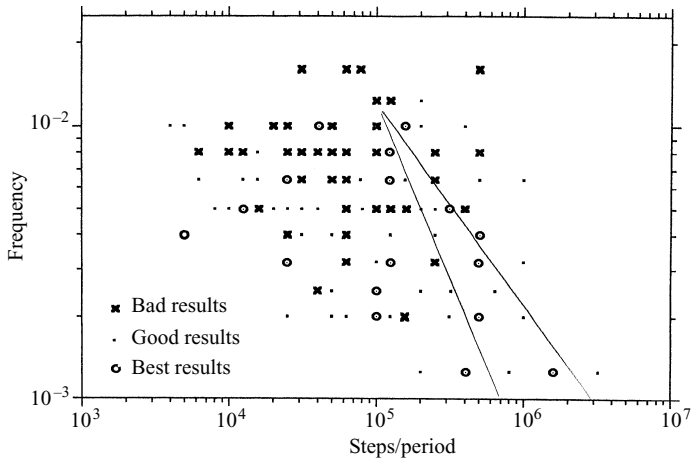


Figure 5. 'Quality' of the stroboscopic trajectories obtained with a third-order symplectic integrator for a GC trajectory starting at $x = y = 0.15$ at time $t = 0$ and represented in the parameter space of wave frequency and integration time step.

are more uniformly distributed in the parameter space. The results are thus more 'unstable' than with the Runge–Kutta (this effect could be due to the order of the integrator being 3 instead of 4 for the Runge–Kutta). We also observe that for small values of the number of steps per period, the two stroboscopic trajectories are not always nicely drawn: the dispersion of the stroboscopic points is important. The best results are therefore more often obtained for small time steps. Concerning the relation between frequency and time step, Fig. 5 shows an oblique line for the 'best' result, whose slope is closer to the expected value of -1. The number of points on the inner stroboscopic trajectory is approximatively 11 for 100 stroboscopic points.

4. Conclusions

The numerical solution of the equations of motion for the guiding centre in three electrostatic waves shows the behaviour expected from the analytical results. For the three-wave Hamiltonian (in the special configuration), the expected result is two stroboscopic trajectories in phase space for one initial condition (see Fig. 3). Therefore the analysis of motion for slowly varying Hamiltonians using adiabatic theory and the formula for the statistics of the stroboscopic points are valid over very long time intervals and for a large number of separatrix crossings. The dependence of the shape and the statistics of the stroboscopic trajectories on the wave frequency has been analysed numerically. We have shown that adiabatic motion appears for waves frequencies smaller than $\omega = 0.01$. This result, extrapolated to the diffusion problem, gives $\mathscr{A} = 1250$, which is a much larger value than the values of the turbulence amplitude considered in numerical simulations. The consequence could thus be a new type of scaling law for diffusion in the asymptotic regime appearing beyond the percolation regime. The 'exact' statistics (which are only known asymptotically) of stroboscopic points in phase space obtained over only 100 points roughly follows the probabilities given by the adiabatic theory. However, more work has to be done to increase the precision in the results because of the instability while passing from one integration time step to the next one. This is

https://doi.org/10.1017/S0022377898006679 Published online by Cambridge University Press

observed on Fig. 4. We see that a line of slope -0.7 passes through the best results of the Runge–Kutta integration scheme. On this line, reaching the domain of small time steps and small frequency, the number of stroboscopic points on the inner trajectory is almost constant. Therefore, along this line, the dynamics at one frequency is similar to the dynamics at a smaller frequency, provided that we perform a consistent (here nonlinear) rescaling of the time. The same conclusion is valid for the symplectic integrator, except that the line of 'best' results has a slope of about -1.

All of these results, and the fact that the stroboscopic trajectories are obtained using the symplectic integrator with time steps that are considered as bad for the Runge–Kutta, show that the Runge–Kutta and symplectic integrators do not work in the same way. The choice of integration scheme could thus have an influence on the numerical results in many problems where long-term behaviour is important.

Acknowledgements

I am grateful to Dr J. Misguich for many stimulating discussions. I take the opportunity of this publication to thank Professor Radu Balescu not only for the pleasure I have had and I still have in learning physics and so many other things from him, but also for his generosity and kindness, which he has constantly provided over the many years we have worked together.

Appendix A. The dimensionless turbulence amplitude

The definitions of various parameters concerning electrostatic turbulence are given here. They are needed to give the scales of the numerical simulations and can be used to relate our parameters to those used in previous works.

The $\mathbf{E} \times \mathbf{B}$ GC motion we consider follows the trajectories of a $1\frac{1}{2}$-degree-of-freedom Hamiltonian:

$$H(x, y, t) = \frac{c}{B}\Phi(x, y, t). \tag{A 1}$$

In the numerical test-particle simulations of the diffusion, the electrostatic potential is given as a sum of random-phase waves (for a recent discussion see Reuss and Misguich 1997):

$$\Phi(x, y, t) = \frac{a_I}{2\pi} \sum_m \sum_n p_{m,n} \sin\left[\frac{2\pi}{L}(mx + ny) - \phi_{m,n} - \omega_0 t\right]. \tag{A 2}$$

In our special configuration of three electrostatic waves, the parameters are

$$\phi_{m,n} = 1, \quad a_I = 2\pi\frac{B}{c}, \quad L = 1, \quad p_{m,n} = 1, \quad w_0 = 2\pi\omega, \tag{A 3}$$

together with the three pairs $(m, n) = (1, 0)$, $(0, 1)$ and $(1, 1)$. The average energy density is thus

$$\mathscr{E} = \frac{1}{8\pi L^2} \int_0^L dx \int_0^L dy\, E^2(x, y, t) \equiv \frac{a_I^2}{8\pi L^2}\sigma_I^2, \tag{A 4}$$

where $\mathbf{E} = -\boldsymbol{\nabla}\Phi$ is the electric field and

$$\sigma_I^2 = \sum_m \sum_n p_{m,n}(n^2 + m^2) = 4. \tag{A 5}$$

https://doi.org/10.1017/S0022377898006679 Published online by Cambridge University Press

The r.m.s electric field $\tilde{E}$ is

$$\tilde{E} = (8\pi\mathscr{E})^{1/2} = \frac{a_I}{L}\sigma_I = \frac{4\pi B}{c}. \tag{A 6}$$

Finally, writing the equations of motion in dimensionless units $x' = x/L$ and $t' = \omega_0 t/2\pi$, we get

$$\frac{d\mathbf{x}'}{dt'} = \frac{2\pi}{L\omega_0}\frac{c\tilde{E}}{B}\,\mathbf{E}(x', y', t') \times \mathbf{b} = \mathscr{A}\,\mathbf{E}(x', y', t') \times \mathbf{b}. \tag{A 7}$$

Obviously, for our three-wave system,

$$\mathscr{A} = \frac{2\pi}{\omega_0 L}\frac{c\tilde{E}}{B} = \frac{4\pi}{\omega}. \tag{A 8}$$

Appendix B. A symplectic integrator

It is instructive to recall the method of building symplectic integrators (more details will be given in Weyssow and Eberhard 1998). A symplectic integrator is a canonical transformation: it is therefore intended for solving specifically Hamilton's equations of motion. The elements of this canonical transformation are an approximate expression of the given Hamiltonian and a 'clock' (needed to define an evolution). The numerical Hamiltonian $H_{\rm num}$ approximates the given Hamiltonian $H(q, p)$ by

$$H_{\rm num}(q, p, \tau, \Delta) = H(q, p) + \sum_{n=1}^{\infty} \tau^n H_n(q, p) + \Delta,$$

where $H(q, p)$ is the initial Hamiltonian. (Note that it is written here as a time-independent Hamiltonian. Such a form can always be obtained by working in a extended phase space). Together with this Hamiltonian, we define the non-vanishing Poisson brackets

$$[q, p] = 1,\ [\tau, \Delta] = 1. \tag{B 1}$$

We also define the Hamiltonian of the 'clock' by

$$H(q_0, p_0, \tau, \delta) = \delta, \tag{B 2}$$

together with the non-vanishing Poisson brackets

$$[q_0, p_0] = 1,\ [\tau, \delta] = 1 \tag{B 3}$$

The canonical transformation defining the symplectic integrator is defined as a near-identity transformation from the approximate Hamiltonian to the 'clock' Hamiltonian:

$$q = q_0 + \tilde{Q}(\tilde{q}, \tilde{p}, \tau), \tag{B 4a}$$

$$p = p_0 + \tilde{P}(\tilde{q}, \tilde{p}, \tau), \tag{B 4b}$$

$$\tau = \tau, \tag{B 4c}$$

$$\Delta = \delta + \tilde{\Delta}(\tilde{q}, \tilde{p}, \tau), \tag{B 4d}$$

where $\tilde{q} = \tilde{q}(q, q_0, p, p_0) together with \tilde{p} = \tilde{p}(q, q_0, p, p_0)$ define the internal stage of the integrator. This transformation is in general implicit, and can be made explicit for separable Hamiltonians. To get a symplectic integrator, we further have to specify

https://doi.org/10.1017/S0022377898006679 Published online by Cambridge University Press

the functional form of the internal stage. For simplicity, we choose the following linear form (Weyssow and Eberhard 1998):

$$\tilde{q} = nq + (1-n)q_0, \ \tilde{p} = (1-n)p + np_0. \tag{B 5}$$

The order of the integrator is the power of τ at which the expansions in τ of the functions $\tilde{Q}(\tilde{q}, \tilde{p}, \tau)$ and $\tilde{P}(\tilde{q}, \tilde{p}, \tau)$ are truncated. Following this procedure, the third-order symplectic integrator reads

$$\begin{aligned} q = q_0 &+ \tau Q - (\tfrac{1}{2} - n)\tau^2(Q\partial_q Q + P\partial_p Q) \\ &- \tau^3\{a_1(Q\partial_q Q\partial_q Q + P\partial_p P\partial_p Q - QP\partial_q\partial_p Q) \\ &+ a_2(QQ\partial_q\partial_q Q + PP\partial_p\partial_p Q) - a_3(Q\partial_q P\partial_p Q + P\partial_p Q\partial_q Q)\}, \end{aligned} \tag{B 6a}$$

$$\begin{aligned} p = p_0 &+ \tau P + (\tfrac{1}{2} - n)\tau^2(Q\partial_q P + P\partial_p P) \\ &- \tau^3\{a_1(Q\partial_q Q\partial_q P + P\partial_p P\partial_p P - QP\partial_q\partial_p P) \\ &+ a_2(QQ\partial_q\partial_q P + PP\partial_p\partial_p P) - a_3(Q\partial_q P\partial_p P + P\partial_p Q\partial_q P)\}, \end{aligned} \tag{B 6b}$$

where

$$Q(q,p) = \frac{\partial H(q,p)}{\partial p}, \quad P(q,p) = -\frac{\partial H(q,p)}{\partial q}, \tag{B 7}$$

and

$$a_1 = \tfrac{1}{6}(6n^2 - 6n + 1), \tag{B 8a}$$

$$a_2 = \tfrac{1}{6}(3n^2 - 3n + 1), \tag{B 8b}$$

$$a_3 = \tfrac{1}{6}(6n^2 - 6n + 2). \tag{B 8c}$$

The internal stage replaces the coordinates (q, p) after the derivatives have been performed. This third-order symplectic integrator is only an example of the many possible symplectic integrators. It has the form of a Taylor method because of the choice of the functional form of the internal stage. We shall always work with $n = \frac{1}{2}$, because in this case, the integration of the equations of motion of the Harmonic oscillator exactly conserves the energy. This is not the case for other values of n.

References

Doxas, I., Horton, W. and Berk, H. L. 1990 Stochastic diffusion in two-dimensional periodic flows. *Phys. Fluids* **A2**, 1906–1909.

Dupree, T. H. 1967 Nonlinear theory of drift-wave turbulence and enhanced diffusion. *Phys. Fluids* **10**, 1049–1055.

Gruzinov, A. V., Isichenko, M. B. and Kalda, Ya. L. 1990 Two-dimensional turbulent diffusion. *Soviet Phys. JETP* **70**, 263–269.

Isichenko, M. B. and Horton, W. 1991 Scaling laws of stochastic $E \times B$ plasma transport. *Comments Plasma Phys. Contr. Fusion* **14**, 249–262.

Misguich, J.-H. and Nakach, R. 1991 Chaotic diffusion across magnetic field in electrostatic three-waves dynamical systems. *Phys. Rev.* **A44**, 3869–3888.

Neistadt, A. I. 1986 Change in adiabatic invariant at a separatrix. *Soviet J. Plasma Phys.* **12**, 568–573.

Ottaviani, M. 1992 Scaling laws of test particle transport in two-dimensional turbulence. *Europhysics Lett.* **20**, 111–116.

Press, W. H., Flannery, B. P., Teukolsky, S. A. and Vetterling, W. T. 1987 *Numerical Recipes*. Cambridge University Press.

https://doi.org/10.1017/S0022377898006679 Published online by Cambridge University Press

Reuss, J.-D. and Misguich, J. H. 1997 Low-frequency percolation scaling for particle diffusion in electrostatic turbulence. *Phys. Rev.* **E54**, 1857–1869.

Weyssow, B. 1997 Guiding centre motion in three electrostatic waves: a pedagogical example for studying adiabatic motions. *Phys. Lett.* **232A**, 234–242.

Weyssow, B. and Eberhard, M. 1998 Symplectic integration revisited (in preparation).

https://doi.org/10.1017/S0022377898006679 Published online by Cambridge University Press